

Interplay between electron band-anticrossing and charge-density-wave instabilities

P.D. Grigoriev^{1,2,3}, A.A. Sinchenko^{4,5}, P.A. Vorobyev⁴, A. Hadj-Azzem⁶, P. Lejay⁶, A. Bosak⁷ and P. Monceau⁶

¹*L. D. Landau Institute for Theoretical Physics, 142432, Chernogolovka, Russia*

²*National University of Science and Technology "MISiS", 119049 Moscow, Russia*

³*P.N. Lebedev Physical Institute, RAS, 119991, Moscow, Russia*

⁴*M.V. Lomonosov Moscow State University, 119991, Moscow, Russia*

⁵*Kotelnikov Institute of Radioengineering and Electronics of RAS, 125009, Moscow, Russia*

⁶*Univ. Grenoble Alpes, Inst. Neel, F-38042 Grenoble,*

France, CNRS, Inst. Neel, F-38042 Grenoble, France and

⁷*ESRF - The European Synchrotron, 71, Avenue des Martyrs, F-38000 Grenoble, France*

(Dated: January 4, 2022)

Our measurements of the Hall coefficient in rare-earth tritelluride compounds reveal a strong hysteresis between cooling and warming in the low temperature range where a second unidirectional charge density wave (CDW) occurs. We show that this effect results from the interplay between two instabilities: band crossing of the Te p_x and p_y orbitals at the Fermi level and CDW, which have a close energy gain and compete. Calculation of the electron susceptibility at the CDW wave vector with and without band anticrossing reconstruction of the electron spectrum yields a satisfactory estimation of the temperature range of the hysteresis in Hall effect measurements.

PACS numbers: 71.45.Lr, 72.15.G-d, 71.18.+y

Crossing of electron energy bands near the Fermi level, resulting in the degeneracy and anticrossing of energy levels, always leads to amazing physical properties. The anticrossing of spin-split energy bands with spin-orbit coupling produces non-trivial topologically-protected electron states in Weyl and Dirac semimetals, which is a subject of extensive research last decade [1–4]. Even without spin effects, the band anticrossing near the Fermi level modifies the electron spectrum and the Fermi surface (FS). This affects various electronic instabilities such as, superconductivity in high-temperature cuprate superconductors [5–7] and spin- or charge-density waves [8–10]. In this paper we unveil the competition of band anticrossing and the charge-density wave (CDW) in the family of rare-earth tritelluride compounds. We show, both theoretically and experimentally, that this interplay leads to the hysteretic electronic phase transition with the change of FS topology and of Hall coefficient.

Layered compounds of $R\text{Te}_3$ family (R =rare earth atom) have a weakly orthorhombic crystal structure (space group $Cmcm$). These systems exhibit an incommensurate CDW through the whole R series [8, 11, 12], with a wave vector $\mathbf{Q}_{CDW1} = (0, 0, \sim 2/7c^*)$ and a Peierls transition temperature above 300 K for the light atoms (La, Ce, Nd). For the heavier R (Tb, Dy, Ho, Er, Tm) a second CDW occurs at low temperature with the wave vector $\mathbf{Q}_{CDW2} = (\sim 2/7a^*, 0, 0)$ perpendicular to \mathbf{Q}_{CDW1} .

For our study we chose three compounds from the $R\text{Te}_3$ family: two compounds, ErTe_3 and HoTe_3 , demonstrating bidirectional CDW ordering at $T_{CDW1} = 270$ and 283 K and $T_{CDW2} = 160$ and 110 K correspondingly, and TbTe_3 revealing an unidirectional CDW at $T_{CDW} = 336$ K. Single crystals of these compounds were grown by a self-flux technique under purified argon atmo-

sphere as described previously [13]. Thin samples with a typical thickness 1-3 μm having a rectangular shape were prepared by micromechanical exfoliation of relatively thick crystals glued on a sapphire substrate.

The magnetic field was applied parallel to the b axis. The Hall resistance $R_{xy}(B) = [V_{xy}(+B) - V_{xy}(-B)]/I$ was recorded using the van der Pauw method [17], sweeping the field between +6 and -6 T at fixed temperature with a step $\Delta T = 10$ K first by cooling from $T > T_{CDW1}$ down to 4.2 K and after that by warming back.

For all measured compounds R_{xy} is a linear function of B at least for temperatures $T \gtrsim 100$ K (see Supplementary Materials (SM)). So, the Hall constant, $R_H = R_{xy}d/B$, where d is the crystal thickness, is indeed a field-independent quantity. Its temperature dependencies for ErTe_3 , HoTe_3 and TbTe_3 are shown in Fig. 1 (a), (b) and (c) correspondingly. One can see that for ErTe_3 and HoTe_3 R_H demonstrates a strong hysteresis between cooling and warming in the temperature range around the second Peierls transition while $R_H(T)$ is completely reversible for TbTe_3 revealing only a single transition to the CDW state in the studied range of temperature. When measured under cooling and warming the temperature dependence of the resistance $R(T)$ of all three compounds was reversible (see SM). It means that the total number of charge carriers remains near the same under cooling and warming. We see only one explanation of this effect: there are two types of carriers, and the hysteresis observed is attributed to the change in electron-hole balance as a result of the second CDW formation. Such scenario is confirmed by the change of the sign of Hall constant at a certain temperature in HoTe_3 and TbTe_3 .

One can naturally attribute the observed effect to the hysteresis of the CDW wave vector \mathbf{Q}_{CDW} due to its

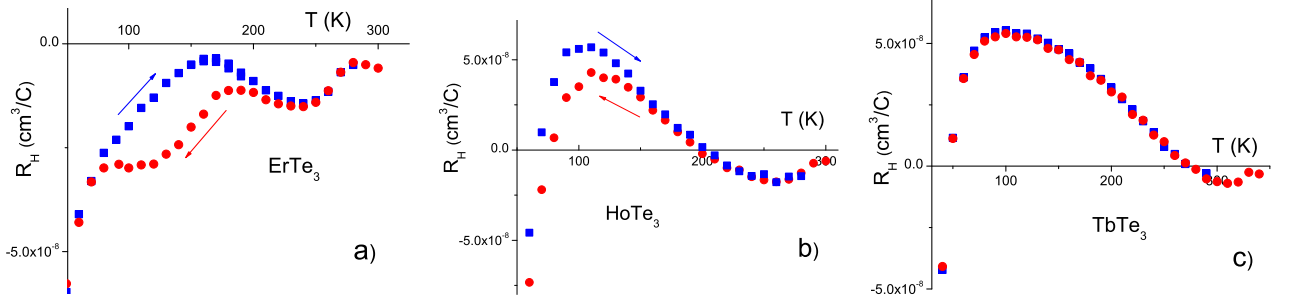


FIG. 1: (color online) Hall constant of ErTe_3 (a), HoTe_3 (b) and TbTe_3 (c) as a function of temperature. Red circles correspond to cooling, and blue squares correspond to warming.

pinning by crystal imperfections. However, our preliminary x-ray diffraction studies of ErTe_3 , performed at ID28 ESRF beamline [14], showed a completely reversible evolution of all structural parameters in the temperature range 100-300 K (see SM). Therefore, we consider another possible origin of this hysteresis, based on the interplay of CDW_2 with another type of electronic instability. As a possible candidate of such electronic ordering competing with CDW_2 , we suggest the one due to the electron band-crossing at the Fermi level.

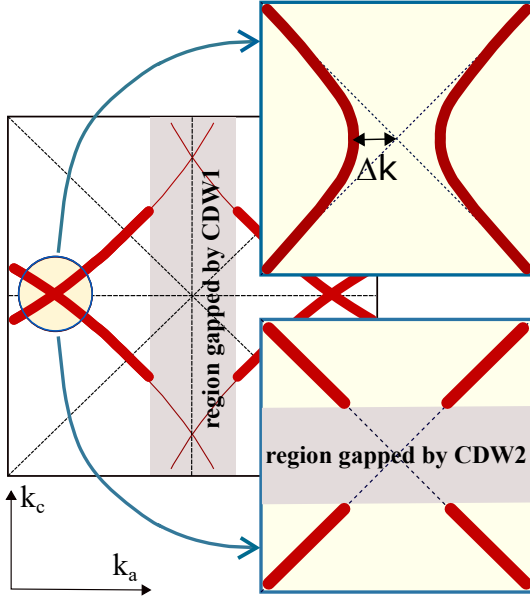


FIG. 2: **Schematic representation of the Fermi surface (FS) in RTe_3 .** Main figure: the full FS with the CDW_1 -gapped region shaded by gray. In the crossing region, highlighted by a filled yellow circle, two FS reconstructions are possible: with band anticrossing shown in the right upper inset, and with energy gap due to CDW_2 shaded by gray in the lower right inset.

Consider two electron bands with electron dispersion $\epsilon_1(\mathbf{k})$ and $\epsilon_2(\mathbf{k})$. Two corresponding Fermi surfaces, given by equations $\epsilon_1(\mathbf{k}) = E_F$ and $\epsilon_2(\mathbf{k}) = E_F$, intersect along the lines $\{\mathbf{k}_0\}$ in the momentum space.

In RTe_3 compounds in the (k_x, k_y) plane below T_{CDW1} there are two such crossing points \mathbf{k}_0 , [18] highlighted by filled yellow circles in Fig. 2. At each degeneracy point \mathbf{k}_0 , any small interband coupling $V(\mathbf{Q})$, even at zero momentum transfer $\mathbf{Q} = 0$, leads to the band anticrossing and to the reconstruction of FS (see right upper inset in Fig. 2). This FS anticrossing has been observed in various RTe_3 compounds by ARPES measurements [12, 16]. The interband coupling $V(\mathbf{Q})$ may originate, e.g., from the electron-electron (e-e) interaction. Usually, $|V(\mathbf{Q})|$ decreases with the increase of momentum transfer $|\mathbf{Q}|$, and $|V(\mathbf{0})| \equiv V_0$ may considerably exceed $|V(\mathbf{Q} \neq \mathbf{0})|$.

First consider the toy model with the interband coupling (off-diagonal terms) only at $\mathbf{Q} = 0$. In this model the different momenta are not coupled, and the Hamiltonian writes down as a sum over electron momenta \mathbf{k} , $\hat{H} = \sum_{\mathbf{k}} \hat{H}_{\mathbf{k}}$, where in the basis of two branches $\alpha = 1, 2$ of electron spectrum each term $\hat{H}_{\mathbf{k}}$ is given by a 2×2 matrix [19]

$$\hat{H}_{\mathbf{k}} = \begin{pmatrix} \epsilon_1(\mathbf{k}) & V_0 \\ V_0 & \epsilon_2(\mathbf{k}) \end{pmatrix} \quad (1)$$

with two eigenvalues

$$E_{\pm}(\mathbf{k}) = \frac{\epsilon_1(\mathbf{k}) + \epsilon_2(\mathbf{k})}{2} \pm \sqrt{\left(\frac{\epsilon_1(\mathbf{k}) - \epsilon_2(\mathbf{k})}{2}\right)^2 + V_0^2}, \quad (2)$$

representing two new branches of electron spectrum. The total electron energy is given by the sum of quasiparticle energies over their quantum numbers:

$$\mathcal{E} = \sum_{\mathbf{k}, \alpha} E_{\alpha}(\mathbf{k}) n_F[E_{\alpha}(\mathbf{k})], \quad (3)$$

where $n_F(\varepsilon) = 1/(1 + \exp[(\varepsilon - E_F)/T])$ is the Fermi-Dirac distribution function. Without band anticrossing the total energy \mathcal{E}_0 is given by the same Eq. (3) with the replacement $E_{\alpha}(\mathbf{k}) \rightarrow \epsilon_{\alpha}(\mathbf{k})$. The difference $\Delta\mathcal{E}_{AC} = \mathcal{E} - \mathcal{E}_0$ comes mainly from the vicinity of the crossing points \mathbf{k}_0 , where two conditions are satisfied: (i) $|\epsilon_1(\mathbf{k}) - \epsilon_2(\mathbf{k})| \lesssim V_0$, so that the electron spectrum changes considerably, and (ii) $|\epsilon_1(\mathbf{k}) + \epsilon_2(\mathbf{k})| \lesssim 2V_0$, so

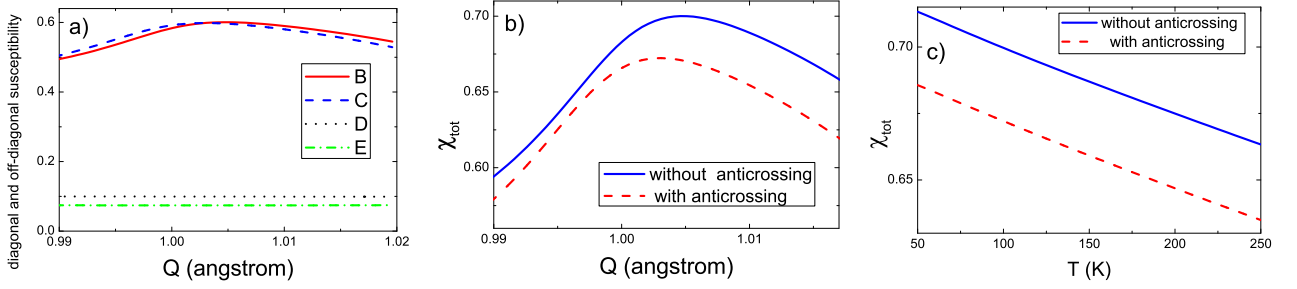


FIG. 3: **Calculated electron susceptibility.** (a) The electron susceptibility contributions without (solid blue and green lines) and with the band-crossing reconstruction (dashed red and black lines). The upper two curves (blue and red) show the calculated "diagonal" intraband contributions χ , while two lower curves (green and black) show "off-diagonal" interband contributions $\Delta\chi$ to susceptibility. (b) Total susceptibility $\chi_{\text{total}} = \chi + \Delta\chi$ as a function of wave vector Q_x near its maximum without (solid blue line) and with the band-crossing reconstruction (dashed red line). (c) The temperature dependence of maximal total susceptibility without (solid blue line) and with the band-crossing reconstruction (dashed red line).

that the change of electron spectrum is close to the Fermi level. Near the crossing point \mathbf{k}_0 one may linearize each branch of electron spectrum:

$$\epsilon_\alpha(\mathbf{k}) \approx v_{F\alpha}(\mathbf{k} - \mathbf{k}_0), \quad (4)$$

where $v_{F\alpha}$ is the Fermi velocity v_F of branch α . Then $|\epsilon_1(\mathbf{k}) \pm \epsilon_2(\mathbf{k})| \approx (v_{F1} \pm v_{F2})(\mathbf{k} - \mathbf{k}_0) \sim v_F |\mathbf{k} - \mathbf{k}_0|$, and the contributing momentum area in the vicinity of the crossing point \mathbf{k}_0 is estimated as $(V_0/v_F)^2$. Then the energy difference per unit area per one spin component but including two cross points is

$$\Delta\mathcal{E}_{AC} \sim -(V_0/\pi\hbar v_F)^2 V_0 \approx -V_0^3 a^2 \rho_F^2, \quad (5)$$

where a is the in-plane lattice constant and $\rho_F = 1/\pi\hbar v_F a$ is the quasi-1D density of states (DoS) at the Fermi level per one branch and spin component. Our calculation of $\Delta\mathcal{E}_{AC}$ by the numerical integration according to Eq. (3) confirms the estimate in Eq. (5), giving the $\Delta\mathcal{E}_{AC}$ value 20% less than in Eq. (5).

The CDW energy gain is [15, 23]

$$\Delta\mathcal{E}_{CDW} = -\Delta^2 \rho_F, \quad (6)$$

where Δ is the CDW energy gap, given by the off-diagonal matrix element of the Hamiltonian, similar to V_0 in Eq. (1). The extra small parameter $\eta \equiv V_0 \rho_F a^2 = V_0 a / \pi\hbar v_F \ll 1$ in the band-crossing energy gain in Eq. (5) as compared to Eq. (6) comes from the small momentum region of contributing electrons, while in a CDW a considerable part of electrons on the Fermi level participate in the Peierls instability, so that a similar small factor $a^2 \rho_F \Delta$ does not appear. Hence, the CDW₂ energy gain may be larger than the energy gain from band anticrossing, although its energy gap $\Delta_2 \ll V_0$.

We estimate the value of V_0 from the FS distortion at the crossing point \mathbf{k}_0 observed in ARPES. This FS distortion Δk along the x -axis is about 3% of the Brillouin zone width $2\pi\hbar/a$, [12, 16] where the lattice constant $a =$

4.28\AA in ErTe₃. This Δk corresponds to the condition $|\epsilon_1(\mathbf{k}) + \epsilon_2(\mathbf{k})| = 2V_0$, giving the boundary of electron states with a gap on the Fermi level according to Eq. (2). In RTe₃ compounds the FS of two bands cross at almost right angle, as shown in Fig. 2. Substituting the electron dispersion (4) with $v_F \approx 1.3 \cdot 10^8 \text{ cm/s}$, we obtain in ErTe₃ compounds $V_0 \approx v_F \Delta k / \sqrt{2} \approx 250 \text{ meV}$. For comparison, in ErTe₃ the CDW₁ energy gap $\Delta_1 \approx 175 \text{ meV}$, and the CDW₂ energy gap is $\Delta_2 \approx 55 \text{ meV}$. [20] The parameter $\eta = V_0 a / \pi\hbar v_F \approx 0.04$ is indeed $\ll 1$, and the ratio of energy gains from the band anticrossing and from CDW₂ is $\Delta\mathcal{E}_{AC} / \Delta\mathcal{E}_{CDW_2} \approx \eta V_0^2 / \Delta_2^2 \approx 0.8$, i.e. slightly less than unity. This means a strong temperature-dependent interplay of these two electronic instabilities, making CDW₂ slightly more energetically favorable at low T . However, since $V_0 / \Delta_2 \approx 5 \gg 1$, the band anticrossing appears at much higher temperature than T_{CDW_2} , even higher than T_{CDW_1} .

The band anticrossing and CDW₂ hinder each other, because each of them change the electron spectrum. The CDW₂ creates an energy gap on the Fermi level just at the spots of FS intersection (see lower right inset in Fig. 2), thus suppressing or making irrelevant the band anticrossing. The influence of band anticrossing on CDW₂ is less obvious, because the FS has an approximate nesting property both with and without the band anticrossing. Moreover, our calculation of the DoS with and without band anticrossing gives nearly the same result in both cases. Hence, to substantiate that band anticrossing hinders the CDW₂ instability, we need to compare the electronic susceptibility $\chi(\mathbf{Q}, T)$ at the CDW₂ wave vector \mathbf{Q} in both cases: with and without band anticrossing reconstruction of electron spectrum. The CDW₂ transition temperature T_c is given by the equation [15] $|U\chi(\mathbf{Q}_{\text{max}}, T_c)| = 1$, where \mathbf{Q}_{max} is the wave vector where the susceptibility χ takes a maximum value. The larger is the susceptibility χ , the higher is the CDW transition temperature, because susceptibility increases with the decrease of temperature.

For calculation we use the well-known formula for the static susceptibility of free-electron gas at finite wave vector \mathbf{Q} . Electron spin only leads to a factor 4 in susceptibility, but the summation over band index α must be retained. Then the real part of electron susceptibility is

$$\chi(\mathbf{Q}) = \sum_{\alpha, \alpha'} \int \frac{4d^d \mathbf{k}}{(2\pi)^d} \frac{n_F(E_{\mathbf{k}, \alpha}) - n_F(E_{\mathbf{k}+\mathbf{Q}, \alpha'})}{E_{\mathbf{k}+\mathbf{Q}, \alpha'} - E_{\mathbf{k}, \alpha}}, \quad (7)$$

where d is the dimension of space. In $R\text{Te}_3$ compounds under study there are two bands crossing the Fermi level, $\alpha, \alpha' = 1, 2$, and we may take $d = 2$ because the dispersion in the z -direction is weak. Eq. (7) differs only by the summation over α and α' from the common expression, e.g., given in Eq. (1.7) of Ref. [15].

Taking the tight-binding bare electron dispersion $\epsilon_{1,2}(\mathbf{k})$ commonly used[9, 22] for $R\text{Te}_3$ compounds and given by Eqs. (2) of Ref. [22], we calculate the susceptibility in Eq. (7) as a function of the wave vector \mathbf{Q} and temperature T for two cases: without band-crossing effect, i.e. for bare electron dispersion $\epsilon_{1,2}(\mathbf{k})$, and for reconstructed dispersion given by Eq. (2). The results are shown in Fig. 3. The integration over momentum in Eq. (7) is performed only at $k_x > k_{x0} \approx 0.29\text{\AA}^{-1}$, because in the momentum region $|k_x| < k_{x0}$ the electron spectrum at the Fermi level has a large gap Δ_1 due to the CDW_1 . The summation over α and α' in Eq. (7) gives four terms: two intraband terms χ with $\alpha = \alpha'$ and two interband terms $\Delta\chi$ with $\alpha \neq \alpha'$. The intraband "diagonal" terms, enhanced by a rather good FS nesting, are much larger than the "off-diagonal" interband terms, because the latter correspond to almost perpendicular FS sheets and do not have such nesting enhancement (see Fig. 3a). Hence, the intraband contribution, shown by upper blue and red curves in Fig. 3a, have a maximum at the CDW_2 wave vector \mathbf{Q} , resulting to a similar maximum on the total susceptibility in Fig. 3b, while the interband contribution, shown by lower green and black curves in Fig. 3a, depends weakly on \mathbf{Q} . Nevertheless, the interband contribution is considerable, being about 20% of the intraband susceptibility. While the maximum values of "diagonal" intraband susceptibility terms are weakly affected by the band anticrossing, the "off-diagonal" interband terms are suppressed by the band anticrossing reconstruction by more than 20% (see Fig. 3a). This can be easily understood by looking at the FS with and without band anticrossing, shown in Fig. 2. The DoS and the nesting property is not violated by the band anticrossing, hence, the intraband terms remain almost the same (only the optimal CDW_2 wave vector slightly shifts). On the contrary, after the band anticrossing reconstruction, the FS of different bands become separated by $\Delta k \sim 3\%$ of the Brillouin zone. Two FS sheets even do not intersect as was without the band anticrossing. Hence, the interband susceptibility decreases considerably.

We have shown that the band anticrossing and CDW_2

interfere, suppressing each other. With temperature decrease the band anticrossing appears first (at higher temperature) and reduces the CDW_2 transition temperature to its observed value T_{CDW_2} . At lower temperature, when CDW_2 develops and the Δ_2 increases, since $|\Delta\mathcal{E}_{\text{CDW}_2}| > |\Delta E_{\text{AC}}|$, the band anticrossing shrinks in favor of CDW_2 . This may happen as a first-order phase transition, accompanied by a hysteresis. When the temperature increases again, the CDW_2 disappears at temperature $T_{\text{CDW}_2}^* > T_{\text{CDW}_2}$, because of the changed band-crossing energy spectrum. This results to a hysteresis seen by the Hall coefficient sensitive to the FS reconstruction due to CDW_2 . We can estimate how strong is this hysteresis by looking at the calculated temperature dependence of susceptibility $\chi(T)$, shown in Fig. 3c. The calculated optimal wave vector \mathbf{Q} of the CDW_2 instability, i.e. of the susceptibility maximum shown in Fig. 3b, very slightly increases with temperature from $Q_x \approx 1.004\text{\AA}^{-1}$ at $T = 50\text{K}$ to $Q_x \approx 1.006\text{\AA}^{-1}$ at $T = 200\text{K}$. Therefore, this change was not observed in X-ray experiment (see SM). In Fig. 3c we plot the maximum value of $\chi(\mathbf{Q})$ as a function of temperature T without (solid blue line) and with (dashed red line) band-crossing reconstruction. They differ by 4.5% only, but since the temperature dependence of susceptibility is also quite weak, the susceptibility value $\chi_c = 0.68$, which the red curve reaches only at $T_c \approx 50\text{K}$, the blue curve has already at $T_c^* \approx 175\text{K}$. Thus, the expected temperature hysteresis is rather large: $\Delta T = T_c^* - T_c \approx 125\text{K}$.

The proposed interplay between band-crossing and CDW is rather general and is expected in many other compounds with FS intersection at the nested parts. For example, similar effect is expected in $R\text{Te}_4$ family of compounds, where a large temperature hysteresis of resistance $\Delta T > 100\text{K}$ has also been observed recently[10].

The bilayer splitting of electron spectrum smears the nesting condition.[20] The exact bare electron dispersion $\epsilon_{1,2}(\mathbf{k})$ are unknown. The coupling between two CDWs in the above analysis is taken into account only by neglecting the contribution from the states gapped by CDW_1 . These and other factors make the interplay of CDW_2 with other instabilities more complicated, but we expect that the main features of the proposed model remain valid.

To summarize, we observed a strong hysteresis of the Hall coefficient in the rare-earth tritelluride compounds ErTe_3 and HoTe_3 , having two CDW phase transitions. We explain this effect by a strong interplay of the low temperature CDW and the band-anticrossing change of electron spectrum. We estimate of the temperature range of this hysteresis by calculating the electron susceptibility at the CDW_2 wave vector with and without band anticrossing. The interplay between these two instabilities is proposed and investigated for the first time and may be relevant to other compounds where two electron bands cross at the Fermi level.

The authors are grateful to the staff of the ID 28 beam line ESRF. The work was partially supported by joint grant CNRS and Russian State Fund for the Basic Research (No. 17-52-150007) and by the Foundation for Advancement of Theoretical Physics and Mathematics "BASIS". P.V. thanks RFBR grant No. 19-02-01000. P.G. thanks State assignment 0033-2019-0001 "The development of condensed-matter theory". A.S. thanks State assignment IRE RAS.

-
- [1] M.Z. Hasan and C.L. Kane, Rev. Mod. Phys. 82, 3045 (2010).
 - [2] Xiao-Liang Qi and Shou-Cheng Zhang, Rev. Mod. Phys. 83, 1057 (2011).
 - [3] Binghai Yan and Claudia Felser, Annu. Rev. Condens. Matter Phys. 8, 337 (2017).
 - [4] N.P. Armitage, E.J. Mele, and Ashvin Vishwanath, Rev. Mod. Phys. 90, 015001 (2018).
 - [5] E. Razzoli, C. E. Matt, Y. Sassa, M. Mansson, O. Tjernberg, G. Drachuck, M. Monomo, M. Oda, T. Kurosawa, Y. Huang, N.C. Plumb, M. Radovic, A. Keren, L. Patthey, J. Mesot, and M. Shi, Phys. Rev. B **95**, 224504 (2017).
 - [6] M. Horio, K. Hauser, Y. Sassa, Z. Mingazheva, D. Sutter, K. Kramer, A. Cook, E. Nocerino, O. K. Forslund, O. Tjernberg, M. Kobayashi, A. Chikina, N. B. M. Schroeter, J. A. Krieger, T. Schmitt, V. N. Strocov, S. Pyon, T. Takayama, H. Takagi, O. J. Lipscombe, S. M. Hayden, M. Ishikado, H. Eisaki, T. Neupert, M. Mansson, C. E. Matt, and J. Chang, Phys. Rev. Lett. **121**, 077004 (2018).
 - [7] Jason K. Perry and Jamil Tahir-Kheli, Phys. Rev. B **58**, 12323 (1998).
 - [8] N. Ru, C. L. Condon, G. Y. Margulis, K. Y. Shin, J. Laverock, S. B. Dugdale, M. F. Toney, and I. R. Fisher, Phys. Rev. B **77**, 035114 (2008).
 - [9] V. Brouet, W. L. Yang, X. J. Zhou, Z. Hussain, R. G. Moore, R. He, D. H. Lu, Z. X. Shen, J. Laverock, S. B. Dugdale, N. Ru, and I. R. Fisher, Phys. Rev. B **77**, 235104 (2008).
 - [10] D.Wu, Q.M. Liu, S.L. Chen, G.Y. Zhong, J. Su, L.Y. Shi, L. Tong, G. Xu, P. Gao, and N.L. Wang, Phys. Rev. Materials **3** 024002 (2019).
 - [11] M. Lavagnini, H.-M. Eiter, L. Tassini, B. Muschler, R. Hackl, R. Monnier, J.-H. Chu, I. R. Fisher, and L. Degiorgi, Phys. Rev. B **81**, 081101(R) (2010).
 - [12] R. G. Moore, V. Brouet, R. He, D. H. Lu, N. Ru, J.-H. Chu, I. R. Fisher, and Z.-X. Shen, Phys. Rev. B **81**, 073102 (2010).
 - [13] A.A. Sinchenko, P. Lejay, and P. Monceau, Phys. Rev. B **85**, 241104(R) (2012).
 - [14] A. Girard, T. Nguyen-Thanh, S. M. Souliou, M. Stekiel, W. Morgenroth, L. Paolasini, A. Minelli, D. Gambetti, B. Winkler and A. Bosak, Journal of Synchrotron Radiation **26**, 272 (2019).
 - [15] G. Grüner, *Density waves in Solids* Perseus Publishing; 1st edition (January 15, 2000).
 - [16] F. Schmitt et al., Science **321**, 1649 (2008).
 - [17] L.J. van der Pauw, Philips Res. Repts. **16**, 187 (1961).
 - [18] Above T_{CDW1} there are 4 crossing points, but two of them disappear after the CDW₁ energy gap opens.
 - [19] In the second-quantization formalism this Hamiltonian writes down as $\hat{H}_{\mathbf{k}} = \epsilon_1(\mathbf{k}) a_1^\dagger(\mathbf{k}) a_1(\mathbf{k}) + \epsilon_2(\mathbf{k}) a_2^\dagger(\mathbf{k}) a_2(\mathbf{k}) + V a_2^\dagger(\mathbf{k}) a_1(\mathbf{k}) + V^* a_1^\dagger(\mathbf{k}) a_2(\mathbf{k})$.
 - [20] B. F. Hu, B. Cheng, R. H. Yuan, T. Dong, and N. L. Wang, Phys. Rev. B **90**, 085105 (2014).
 - [21] L. D. Landau and E. M. Lifshitz, Course of Theoretical Physics, Vol. 5: Statistical Physics, 3rd ed. (Nauka, Moscow, 1976; Pergamon Press, Oxford, 1980).
 - [22] A.A. Sinchenko, P.D. Grigoriev, P. Lejay and P. Monceau, Phys. Rev. Lett. **112** 036601 (2014).
 - [23] The extra factor 2 comes from the summation over two bands.

Supplementary information on "Interplay between electron band-crossing and charge-density-wave instabilities"

P.D. Grigoriev^{1,2,3}, A.A. Sinchenko^{4,5}, P.A. Vorobyev⁴,
A. Hadj-Azzem⁶, P. Lejay⁶, A. Bosak⁷ and P. Monceau⁶

¹*L. D. Landau Institute for Theoretical Physics, 142432, Chernogolovka, Russia*

²*National University of Science and Technology "MISiS", 119049 Moscow, Russia*

³*P.N. Lebedev Physical Institute, RAS, 119991, Moscow, Russia*

⁴*M.V. Lomonosov Moscow State University, 119991, Moscow, Russia*

⁵*Kotelnikov Institute of Radioengineering and Electronics of RAS, 125009, Moscow, Russia*

⁶*Univ. Grenoble Alpes, Inst. Neel, F-38042 Grenoble,
France, CNRS, Inst. Neel, F-38042 Grenoble, France and*

⁷*ESRF - The European Synchrotron, 71,
Avenue des Martyrs, F-38000 Grenoble, France*

(Dated: January 4, 2022)

HALL EFFECT MEASUREMENTS

Schematic representation of the Hall effect measurements is shown in Fig. 1. The magnetic field was applied parallel to the b axis, and the Hall resistance $R_{xy}(B) = [V_{xy}(+B) - V_{xy}(-B)]/2I$ was recorded using the van der Pauw [1] method, sweeping the field between +6 and -6 T at fixed temperature with a step $\Delta T = 10$ K under the cooling from $T > T_{CDW1}$ up to 4.2 K and after that under warming back.

The shape of a $R\text{Te}_3$ single crystals is a very thin plate with the long b -axis perpendicular to the plane of the plates. Therefore, for Hall effect measurements the chosen experimental geometry is the most convenient.

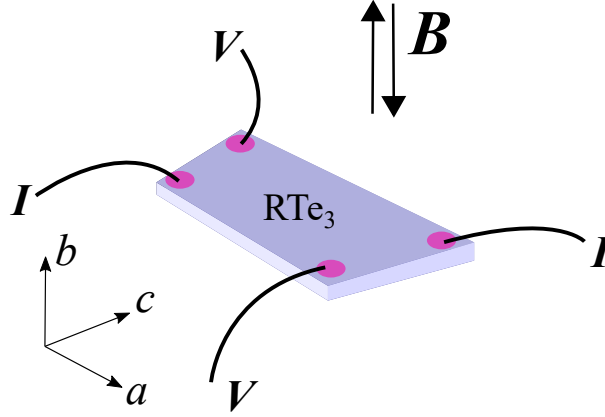


FIG. 1: Schematic representation of the Hall effect measurement with the van der Pauw method

Fig. 2 (a-c) represent the Hall resistance as a function of magnetic field in the temperature range from 4.2 K up to the temperature which is well above T_{CDW1} for all studied compounds. Hall resistance changes sign at a certain temperature in HoTe_3 and TbTe_3 . Such crossing is absent for ErTe_3 although it can be seen that R_H also has a tendency to cross zero near 150-170 K (see Fig.1 (a) in main text). However it is the second CDW transition at $T = 160$ K which interrupts this tendency. Another fact is that the formal estimation of carrier concentration for the case one band gives unrealistic values, of the order $10^{27} - 10^{28} \text{ cm}^{-3}$. All these facts indicate that there are two types of carriers in $R\text{Te}_3$ compounds with near the same concentration of electrons and holes.

Usually in such a system with two (electron and hole) conduction channels, the Hall resistivity as a function of B should be non-linear. In this case $\rho_{xy}(B)$ can be well fitted to a two-band model as,

$$\rho_{xy}(B) = \frac{B}{e} \frac{(n_h \mu_h^2 - n_e \mu_e^2) + (n_h - n_e) \mu_e^2 \mu_h^2 B^2}{e(n_h \mu_h - n_e \mu_e)^2 + [(n_h - n_e) \mu_h \mu_e B]^2} \quad (1)$$

where n and μ are respectively carrier density and mobility, and the subscript e (or h) denotes electron (or hole). As can be seen from Fig. 2 our $R_{xy}(B)$ dependencies are non-linear in the measured magnetic field range but only at low enough temperatures. At higher temperatures (> 100 K) R_{xy} is a nearly linear function of B most probably because low enough carriers mobility. Indeed, as can be seen from equation (1) the non-linearity of $R_{xy}(B)$ is determined mainly by the second term in numerator the value of which strongly depends on carrier mobilities. Estimation from magnetoresistance [2] gives for $(\mu_e \mu_h) \sim 10^3 \text{ cm}^4/\text{V}^2\text{s}^2$ that is really small. It can be expected that at higher magnetic field the non-linearity of $R_{xy}(B)$ will be observable at high temperature also. In the case of the present experiment we can consider the Hall constant, $R_H = R_{xy}d$, where d is the crystal thickness, as a real constant value at $T > 100$ K.

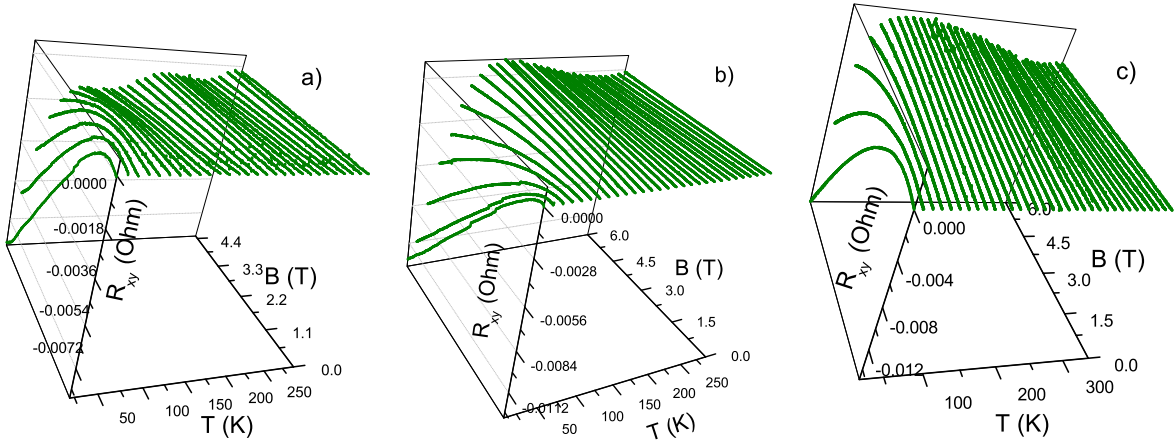


FIG. 2: Hall resistance, R_{xy} as a function of temperature and magnetic field of ErTe_3 (a), HoTe_3 (b) and TbTe_3 (c) under cooling.

RESISTIVITY

The resistivity singularity corresponding to the second CDW transition is very weak in $R\text{Te}_3$ compounds and most often can be resolved only in the derivative $dR/dT(T)$. Fig.3 (a) shows example of such dependency for ErTe_3 . Fig.3 (b) and (c) demonstrate the behavior of resistance of ErTe_3 and HoTe_3 samples shown in Fig.1 in main text under cooling and

warming in the temperature range corresponding to the second CDW transition. Each point was taken at fixed T as $R = V(B = 0)/I$. As can be seen, this dependence is reversible in the limit of experimental error.

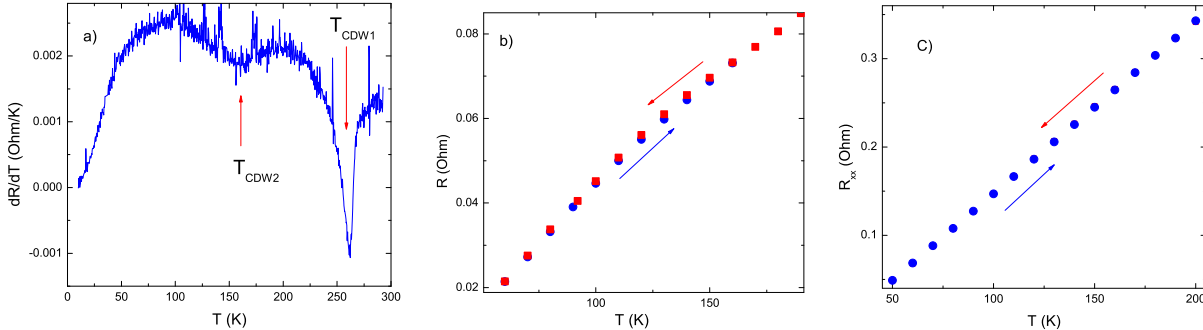


FIG. 3: (a) dR/dT as a function of temperature for ErTe_3 . (b) and (c) temperature dependence of resistance of ErTe_3 and HoTe_3 under cooling (red) and warming (blue).

X-RAY DIFFRACTION

The diffraction measurements were carried out on the side station of the ID28 beamline of the European Synchrotron Radiation Facility (ESRF). We used a monochromatic beam with wavelength of 0.6968 \AA . The frames were acquired with a Pilatus 3X 1M detector in shutterless mode with the angular step of 0.25 deg for several temperatures between room temperature (RT) and 90 K. The sample temperature was controlled by the Oxford Cryosystems Cryotream 700 Plus. Orientation matrix refinement and preliminary reciprocal space reconstructions were performed using the CrysAlis software package, final reconstructions are produced with locally developed software.

No visible difference was found neither in the intensities of modulation spots nor in the diffuse scattering component for heating and cooling, as illustrated by the reconstructions of $h0l$, $3kl$ and $hk3$ planes shown for 160 K.

[1] L.J. van der Pauw, Philips Res. Repts. **16**, 187 (1961).

[2] A. A. Sinchenko, P. D. Grigoriev, P. Lejay, and P. Monceau, Phys. Rev. B **96**, 245129 (2017).

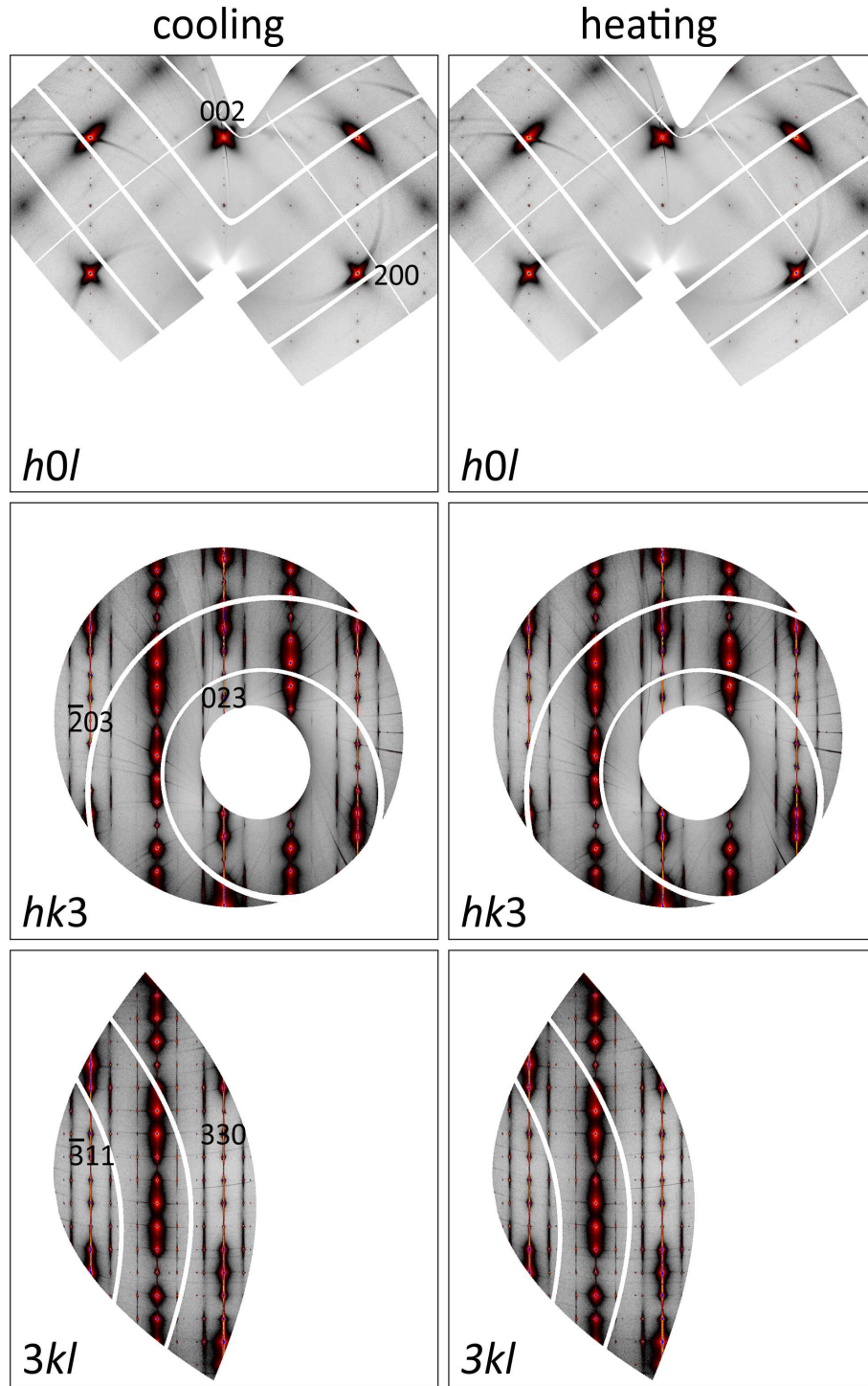


FIG. 4: Reciprocal space planes $h0l$, $3kl$ and $hk3$ of ErTe_3 as reconstructed for 160K on cooling from room temperature and as on heating from 90 K.